Cilt 12, Sayı 1, Sayfa 144-152, 2023 Volume 12, Issue 1, Page 144-152, 2023

Araştırma Makalesi https://doi.org/10.46810/tdfd.1250042 Research Article

BİNGÖL ÜNİVERSİTESİ

Türk Doğa ve Fen Dergisi
Turkish Journal of Nature and Science
www.dergipark.gov.tr/tdfd

# The Study of 2, 4-Diamino-6-methly-1, 3, 5-triazine on the Corrosion Inhibition of Mild Steel in The Hydrochloric Acid Medium: Integrated Theoretical and Experimental Investigations

**Reşit YILDIZ[1*]**

[1]Mardin Artuklu University, Faculty of Health Sciences, Department of Nutrition and Dietetics, Mardin, Türkiye
Reşit YILDIZ ORCID No: 0000-0001-5467-6821

[*]Corresponding author: *ryildiz80@gmail.com*, *resityildiz@artuklu.edu.tr*

(Received: 11.02.2023, Accepted: 14.03.2023, Online Publication: 27.03.2023)

**Keywords**
Corrosion,
Adsorption,
Mild steel,
Inhibitor, Quantum chemical calculation,

**Abstract:** The aim of this study is the investigation of adsorption and corrosion behaviors of 2,4-Diamino-6-methly-1,3,5-triazine (2-DMT) on mild steel (MS) in 0.5 M HCI solution using many experimental and theoretical studies such as potentiodynamic polarization, electrochemical impedance spectroscopy (EIS), linear polarization resistance (LPR), adsorption isotherm, potential of zero charge (PZC), scanning electron (SEM), atomic force microscopies (AFM) and quantum chemical calculations. The results showed that 2-DMT has an outstanding anti-corrosion performance of 94.7% at an optimum concentration of 10 mM and the MS surface, which was exposed to the inhibited solution at 298 K, does not contain pits, cracks or deformations. Values of $i_{corr}$ are found to be 0.513, 0.216, 0.098, 0.072 and 0.039 mA cm$^{-2}$ for blank solution and each concentration of 2-DMT. Hydrogen volumes are 90 and 4.6 mL cm$^{-2}$ for blank solution and the existence of 10.0 mM 2-DMT, respectively. The observed adsorption is much more consistent with Langmuir. The high performance is explained by the effective adsorbing of organic matter to the MS surface. HOMO, LUMO energies and the energy gap ($\Delta E$) are -7.1980, -1.9959 and 5.2021 eV, respectively. Accordingly, it is suggested that this organic compound can be used in the industrial acid cleaning procedure.



# 2, 4-Diamino-6-metil-1, 3, 5-triazinin Yumuşak Çeliğin Hidroklorik Asit Ortamda Korozyon İnhibisyonu Üzerine Çalışması: Teorik ve Deneysel Araştırmaların Bütünleştirilmesi

**Anahtar Kelimeler**
Korozyon,
Adsorbsiyon,
Yumuşak çelik,
İnhibitör,
Kuantum kimyasal hesaplama,

**Öz:** Bu çalışmanın amacı, potansiyodinamik polarizasyon, elektrokimyasal empedans spektroskopisi (EIS), doğrusal polarizasyon direnci (LPR), adsorbsiyon izotermi, sıfır yük potansiyeli (PZC), taramalı elektron (SEM), atomik kuvvet mikroskopileri (AFM) ve kuantum kimyasal hesaplamaları gibi birçok deneysel ve teorik çalışma kullanılarak 0,5 M HCI çözeltisinde 2,4-Diamino-6-methly-1,3,5-triazinin (2-DMT) adsorbsiyon ve korozyon davranışlarının incelenmesidir. Sonuçlar, 2-DMT'nin 10 mM'lik optimum konsantrasyonda % 94,7'lik olağanüstü korozyon önleyici performansa sahip olduğunu ve 298 K'de inhibe edilmiş çözeltiye maruz kalan çelik yüzeyin çukurlar, çatlaklar veya deformasyonlar içermediğini göstermiştir. Asit çözeltisi ve 10 mM 2-DMT varlığındaki çözelti için, $i_{corr}$ değerleri 0,513, 0,216, 0,098, 0,072 ve 0,039 mA cm$^{-2}$ olarak bulundu. Hidrojen hacmi sırasıyla, asit çözeltisi ve 10 mM 2-DMT varlığındaki çözelti için 90 ve 4,6 mL cm$^{-2}$' dir. Gözlemlenen adsorbsiyon, Langmuir ile çok daha tutarlıdır. Yüksek performans, organik maddenin MS yüzeyine etkili bir şekilde adsorbe olmasıyla açıklanmaktadır. HOMO, LUMO enerjileri ve enerji aralığı ($\Delta E$) sırasıyla, -7,1980, -1,9959 ve 5,2021 eV' tur. Dolayısıyla, bu organik bileşiğin endüstriyel asitle temizleme işleminde kullanılabileceği önerilmektedir.

## 1. INTRODUCTION

Corrosion, which has an annual global cost of 2.5 trillion dollars, is defined as the loss of effectiveness of metals as a result of their interactions with their environment [1]. Even if this phenomenon is completely impossible to stop, studies to slow down corrosion continue intensively by many researchers [2-5]. One of the industrial areas where corrosion is effective is acid cleaning, pickling and descaling [6,7]. HCl and $H_2SO_4$ are used to clean the steel materials in this area as cleaning agents, therefore the corrosion is inevitable. Using organic corrosion inhibitors are an effective method in the slow down the corrosion [8-11]. These compounds adsorb on the steel surface effectively, form a protective film on the steel surface and by inhibiting the corrosion reactions, protect the steel from corrosion. This corrosion protection is described in the literature as: Conjugated bonds, polar groups such as N, O, P, S and π-delocalized electrons in inhibitor molecules are adsorption centres during the interaction of metal and inhibitor molecules [12-14]. Many organic compounds as corrosion inhibitors are studied to prevent the different metals as well as MS. As examples, pyrazole, benzimidazole, azoles, pyridine, schiff bases, amino acids, quinoline, quinoxaline, rhodanine, etc. In recent years, triazine derivatives as organic inhibitors showed high inhibition efficiency in acid solutions [15]. Triazine derivatives are also used in the medical field for anti-HIV, anticancer, antiinflammatory, analgesic antihypertensive, cardiotonic, neuroleptic, nootropic, antihistaminergic, tuberculostatic, antiviral, anti-protozoal, estrogen receptor modulators, antimalarial, cyclin-dependent kinase inhibitors, antimicrobial, antiparasitic, activities [16].

In this study, 2,4-Diamino-6-methyl-1,3,5-triazine, a triazine derivative, is tested as a potential organic corrosion inhibitor to specify the corrosion properties of MS in 0.5 M HCI solution using electrochemical techniques, SEM/AFM and quantum chemical calculation. As mentioned above, this compound is chosen as an inhibitor because it contains electron-donating groups and possible adsorption groups in the aromatic ring. Its cost is another reason. Hydrogen gas is also measured in inhibited and uninhibited solutions after 120 h exposure time. The inhibition mechanism is discussed in more detail by determining the charge of metal. Finally, this work is supplemented by quantum chemical calculation to better understand the relationship between structural, electronic properties and adsorption process.

## 2. MATERIAL AND METHOD

The chemical composition of MS used in this study is (w): Mn: 0.71%, Cu: 0.26%, Si: 0.24%, C: 0.18%, S: 0.04%, P: 0.19%, N: 0.20%, O: 0.41% and Fe (remainder). To get a clean surface before electrochemical measurements, emery papers are used, washed with ethanol and distilled water, respectively. The corrosive media is composed by 0.5 M HCI (Merck, 37% HCI) without and with concentrations of 0.5, 1.0, 5.0 and 10.0 mM 2-DMT. Gamry instrument potentiostat/galvanostat/ZRA/3000 is used for electrochemical measurements with three-electrode setup which consists of MS as working, platinum sheet as counter and Ag/AgCI (3M KCI) as reference electrode, respectively. Prior to each experiment, stable open circuit potential ($E_{ocp}$) is achieved after 1 h immersion time in both corrosive solutions. Tafel curves is gotten between -0.75 and -0.25 V with a scan rate of 1 mV $s^{-1}$. Frequency between $1x10^5$ Hz and $1x10^{-2}$ Hz is applied to get EIS diagrams with an amplitude of 5 mV. Moreover, EIS results are fitted by using equivalent circuit with the help of Zview2 software. Measurement of LPR is recorded from $E_{ocp}$ -0.01 V to $E_{ocp}$ +0.01 V at 1.0 mV $s^{-1}$. The effect of various immersion times (24, 48, 72, 96 and 120 h) on corrosion behavior of MS electrode in blank and with the existence of inhibitor (10.0 mM) are examined by EIS. Hydrogen gas is measured by an inverted tape measure at the end of 120 h in both uninhibited and inhibited solutions (10.0 mM). To determine the charge of metal in inhibited solution (10.0 mM) it is plotted polarization resistance ($R_p$) versus applied potential. All the electrochemical experiments are carried out under atmospheric conditions by repeating three times at 298 K. To analyze the morphologic structure and elemental analysis, SEM and AFM are performed by Leo Evo 40 and Park system XE-100 AFM, respectively. Electrochemical results are supplemented by quantum chemical calculation, namely the basis set B3LYP/6-311 ++ G (d, p) for all atoms with the Gaussian 09 program package (USA). Some electronic properties such as the energy of the highest molecular orbital ($E_{HOMO}$), lowest empty molecular orbital ($E_{LUMO}$), energy gap ($\Delta E$) between LUMO and HOMO and Mulliken charges on the backbone atoms, dipole moment ($\mu$), global hardness ($\eta$), global softness ($\sigma$), the fraction of electrons transferred ($\Delta N$) and absolute electronegativity ($\chi$) are determined. The chemical structure of the tested inhibitor is given in Figure 1.

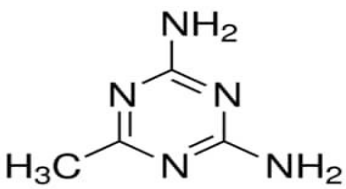


**Figure 1.** Chemical structure of 2,4-Diamino-6-methly-1,3,5-triazine (2-DMT)

## 3. DISCUSSION AND CONCLUSION

### 3.1. Tafel Results

The Tafel curve is the best method for determining of corrosion behavior of MS electrode in acid environment. Fig. 2 shows the Tafel curves of MS electrode in blank solution and with the existence of 0.5, 1.0, 5.0 and 10.0 mM 2-DMT.

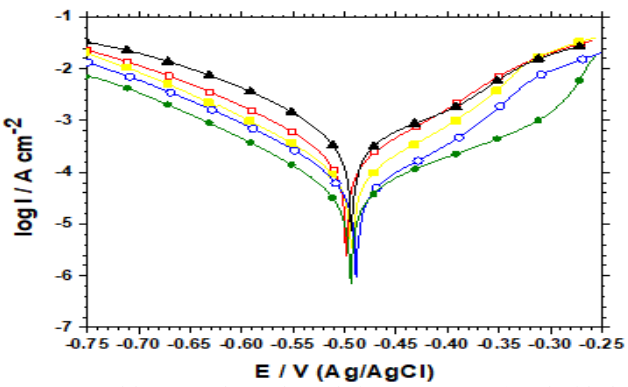


**Figure 2.** Tafel curves of MS electrode in 0.5 M HCI(▲) and with the existence of 0.5(□), 1.0(●), 5.0(○) and 10.0(●) mM 2-DMT

Prior to adding to the inhibitor in 0.5 M HCI solution, Fig. 2 clearly indicates that very high current density is obtained on MS electrode. When an inhibitor is added to a corrosive medium at concentrations of 0.5 to 10 mM, 2-DMT molecules influence the corrosion current density of the cathodic and anodic reactions, resulting in reducing the rate of anodic dissolution of the metal and cathodic reaction [17]. The highest decrease in current density is observed at the highest concentration (10 mM). The Tafel extrapolation method is used for the determination of corrosion current density ($i_{corr}$) and cathodic Tafel slopes ($b_c$). In addition, corrosion rate (CR) and inhibition efficiencies ($\eta$(%)) are also measured and related data are given in Table 1. The following formula is used for $\eta$(%).

$$\eta(\%)=(i^o_{corr}-i_{corr}inh/i^o_{corr})x100 \quad (1)$$

Here, $i^o_{corr}$ and $i_{corr}$ inh denote the corrosion current density of MS electrode in acid environment in the absence and presence of inhibitor, respectively. It is clearly seen from figure that characteristic behavior of Tafel curves does not change with the existence of different concentrations of 2-DMT in blank solution, implying that the same corrosion mechanism occurs in both corrosive media due to giving parallel lines. $b_c$ values support this behavior since there are small differences between MS electrode in blank solution and the existence of an inhibitor in blank solution (Table 1). This means that inhibitor molecules block the active centres of hydrogen evolution by adsorbing on the MS surface for the cathodic region, slow down the anodic dissolution of the MS for anodic region [18]. From Table 1, this inhibitor acts as a mixed-type inhibitor due to a maximum potential difference of 5 mV [19]. As can be seen in Table 1, values of $i_{corr}$ are found to be 0.5128, 0.2155, 0.0983, 0.07151 and 0.03861 mA cm$^{-2}$ for the blank solution and each concentration of 2-DMT. A decrease in $i_{corr}$ indicates the adsorption of inhibitor molecules onto MS surface. As for $\eta$, Table 1 shows the dependency of the inhibition efficiency on the inhibitor concentration. Inhibition efficiency increases from 58% to 92.4% in inhibited solution. This means that a stable inhibitor film forms on the MS surface and this film behaves like a preventative, resulting the reducing $i_{corr}$ values.

**Table 1.** Some data derived from Tafel curves of MS electrode in blank solution and with the existence of different concentrations 2-DMT at 298 K

| $C_{inh}$ (mM) | $E_{corr}$ (mV,Ag/AgCl) | $i_{corr}$ (mA cm$^{-2}$) | $bc$ (mV dec$^{-1}$) | CR (mpy) | $\eta$(%) |
|---|---|---|---|---|---|
| Blank | -493.7 | 0.5128 | 118.3 | 234.3 | - |
| 0.5 | -498.7 | 0.2155 | 108.5 | 98.49 | 58.0 |
| 1.0 | -492.4 | 0.0983 | 101.1 | 44.92 | 80.8 |
| 5.0 | -488.9 | 0.07151 | 102.6 | 32.68 | 86.0 |
| 10.0 | -493.9 | 0.03861 | 100.0 | 17.64 | 92.4 |

### 3.2. EIS and LPR Results

The relationship at the metal/solution interface can be elucidated by EIS. Nyquist and Bode plots of MS electrode in blank solution and with the addition of 0.5, 1.0, 5.0 and 10.0 mM 2-DMT are depicted in Fig. 3. The same shapes (one depressed semicircle) are seen for all electrodes in Bode plots (Fig. 3b), indicating that mechanism is controlled by charge transfer at the interface [20]. The reason why perfect semicircles are not obtained is due to the uneven charge distribution at the interface [21]. Impedance responses are fitted using equivalent circuit that is depicted in Fig. 3b as an inset. A single circuit is used in the fitting process. Because the most suitable fitting is obtained in this circuit. Fitting data are given in Table 2. Here $R_s$, $R_p$, CPE and $n$ denote solution resistance, polarization resistance that is containing charge transfer resistance ($R_{ct}$), diffuse layer resistance ($R_d$), the resistance of accumulated species ($R_a$) and film resistance ($R_f$), constant phase element and phase shift, respectively. The following formula is used for $\eta$.

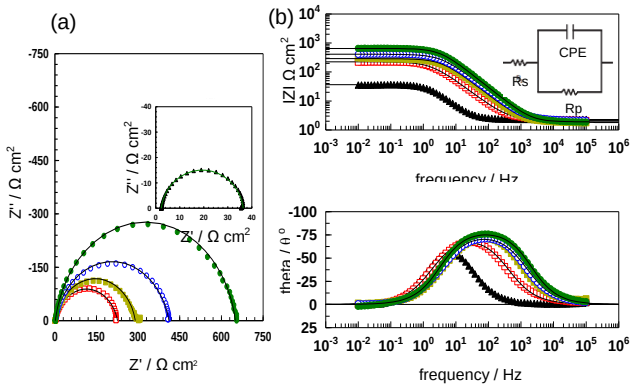


**Figure 3.** Nyquist (a) and Bode (b) plots of MS electrode (▲ or as inset) in 0.5 M HCI and with the existence of 0.5(□), 1.0(■), 5.0(○) and 10.0(●) mM 2-DMT. A related equivalent circuit is given in b as an inset.

**Table 2.** Some data derived from EIS and LPR for MS electrode in blank solution and with the existence of different concentrations 2-DMT at 298 K

| $C_{inh}$ (mM) | EIS | | | | | | | LPR | |
|---|---|---|---|---|---|---|---|---|---|
| | $R_s$ ($\Omega cm^2$) | $R_p$ ($\Omega cm^2$) | $CPE_{dl}$ $Y_o$ ( $x10^6$ $s^n$ $\Omega^{-1}$ $cm^{-2}$) | $n$ | $\eta$ (%) | $C_{dl}$ ($x10^6$ s $\Omega^{-1}$ $cm^{-2}$) | Fit error (chi-squared) | $R_p$ ($\Omega cm^2$) | $\eta$ (%) |
| Blank | 2.3 | 34 | 361 | 0.92 | | 248 | $4.2x10^{-3}$ | 37 | |
| 0.5 | 2.2 | 224 | 255 | 0.86 | 84.8 | 158 | $1.1x10^{-2}$ | 240 | 84.5 |
| 1.0 | 1.8 | 288 | 219 | 0.87 | 88.1 | 152 | $1.0x10^{-2}$ | 310 | 88.0 |
| 5.0 | 2.1 | 409 | 163 | 0.85 | 91.6 | 104 | $6.2x10^{-3}$ | 425 | 91.2 |
| 10.0 | 1.9 | 648 | 102 | 0.90 | 94.7 | 77 | $8.1x10^{-3}$ | 690 | 94.6 |

$$\eta\ \% = \left(\frac{R'_p - R_p}{R'_p}\right) \times 100 \quad (2)$$

$R_p$ and $R'_p$ denote the polarization resistance of MS electrode in blank solution and with the adding of 2-DMT, respectively. To calculate the CPE and double layer capacitance ($C_{dl}$), formulas are given below:

$$Z_{CPE}=Y_o^{-1}(jw)^{-n} \quad (3)$$

where $Y_o$, $j$, $w$ and $n$ are proportionality coefficient, $j^2$ = -1 imaginary number, angular frequency and phase shift, respectively.

$$C_{dl}=Y_o(w''_m)^{n-1} \quad (4)$$

$w''_m = 2\pi f_{max}$ (angular frequency), $f_{max}$ is the frequency at the maximum value of imaginary impedance [22]. As seen in Fig. 3a, the diameter of depressed semicircles which is directly related to $R_p$ values increases regularly with the adding of 0.5, 1.0, 5.0 and 10.0 mM 2-DMT in 0.5 M HCI, when compared to bare MS electrode. The increase in the diameter of the semicircle represents a measure of protection. This is supported by the increasing phase angles in the Bode curves (Fig. 3b). According to Table 2, when the concentration enhances from 0.5 to 10.0 mM, inhibition efficiency reaches its highest value from 84.8% to 94.7%. Here $n$ is related to the non-homogeneous nature of the semicircles which is a characteristic for solid metals [23]. Its value is between 0 and 1. As for $C_{dl}$ values, as expected, $C_{dl}$ values decrease with increasing 2-DMT concentration due to decreasing in the local dielectric constant and increasing the thickness of the double layer [24]. High inhibition efficiency and lower $C_{dl}$ values can be due to adsorption of inhibitor molecules onto the MS surface and by causing a protective layer, preventing the MS from corrosion [25]. Increments of phase angles prove the existence of surface protection (Fig. 3b). In the present work, as seen in Table 2, the results of LPR are very close to the results of EIS. A comparison of the protection ability of some triazine-containing compounds with 2,4-Diamino-6-methly-1,3,5-triazine are given in Table 3. Though researchers found very high inhibition efficiencies, as can be seen in Table 3, the inhibition ability of studied inhibitor is higher than those of the previously studied inhibitors. In general, inhibitors which have protection ability over 80% in acidic medium find place in industrial applications. This promising result once again exhibits the importance of this class of compounds for protecting metals in an acidic medium.

**Table 3.** Comparison of protection ability of 2-DMT with literature

| Inhibitor | Metal | Medium | $\eta$(%) | Ref |
|---|---|---|---|---|
| Triazine-glycine | Mild steel | 1.0 M HCl | 71.2 | [22] |
| 1,3,5-tri-p-tolyl-1,3,5-triazene | Brass | 0.5 M HCl | 76.0 | [26] |
| 6-methyl-5-[m-nitrostyryl]-3-mercapto-1,2,4-triazine | Tubing steel | 12% HCl | 87.1 | [27] |
| $N^2$-(4-(5-(4-methoxyphenyl)isoxazol-3-yl)phenyl)-$N^4$,$N^6$-diphenyl-1,3,5-triazine-2,4,6-triamine | Mild steel | 1 M HCl | 92.0 | [28] |
| 4-amino-6-methyl-3-thioxo-3,4-dihydro-1,2,4-triazin-5(2H)-one | Mild steel | 1.0 N HCl | 92.9 | [29] |
| 1,3,5-tris(4-methoxyphenyl)-1,3,5-triazine | N80 steel | 15% HCl | 93.2 | [30] |
| Hexahydro-1,3,5-p-aminophenyl-s-triazine | Mild steel | 1.0 N HCl | 96.1 | [31] |
| 2,4-Diamino-6-methly-1,3,5-triazine | Mild steel | 0.5 M HCl | 94.7 | This work |

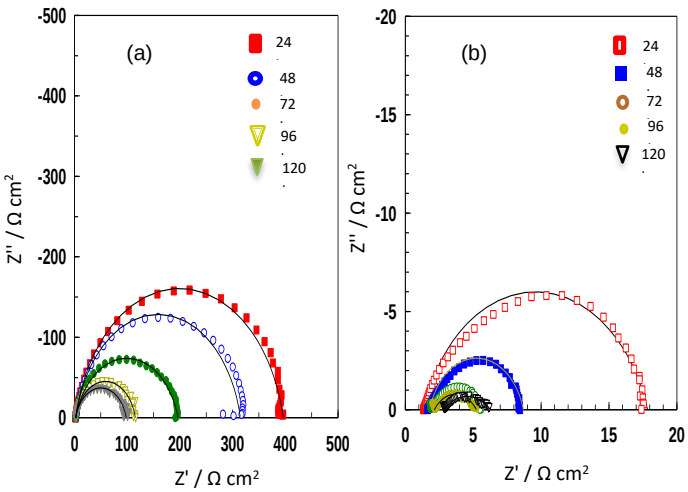


**Figure 4.** Nyquist plots of MS electrode (b) in 0.5 M HCI and with the existence of 10.0 mM 2-DMT (a) after different exposure times. Straight lines show the fitting curves.

Corrosion properties of MS in blank solution and with the existence of 10.0 mM 2-DMT are evaluated using EIS after 24, 48, 72, 96 and 120 h exposure times (long-immersion time) and related Nyquist diagrams are represented in Fig. 4. All EIS responses show the same behavior due to observing one depressed semicircle after long-immersion times. The acid solution damaged the bare MS heavily. Because $R_p$ values decreased from 17.0 $\Omega$ $cm^2$ to 3.3 $\Omega$ $cm^2$. Although polarization resistances decreased from 394 $\Omega$ $cm^2$ to 95 $\Omega$ $cm^2$ with the existence of 10.0 mM 2-DMT, polarization resistances are still higher when compared to those of blank solution results. Long-immersion time results showed that 2-

DMT underlines that it reduces the corrosion rate and the existence of an effective inhibition on the MS surface [32]. Besides, corrosion inhibition efficiencies are also calculated using equation 2, the values changed between 95.6% and 98.0%. LPR method supported by these values. To confirm the results of long-immersion time experiments obtained with EIS and LPR, the volume of hydrogen gas released at the MS electrode was measured at the end of 120 hours via an inverted tape measure and these results are given in Fig. 5. It is clearly seen from Fig. 5, while the hydrogen volume increased at the MS electrode as a result of corrosion, the hydrogen volume increased very slowly in the presence of 2-DMT. Measured volumes are 90 mL cm$^{-2}$ for blank solution and 4.6 mL cm$^{-2}$ for existence of 10.0 mM 2-DMT in 0.5 M HCI, respectively. These results confirm the results of long-immersion time experiments obtained with EIS and LPR.

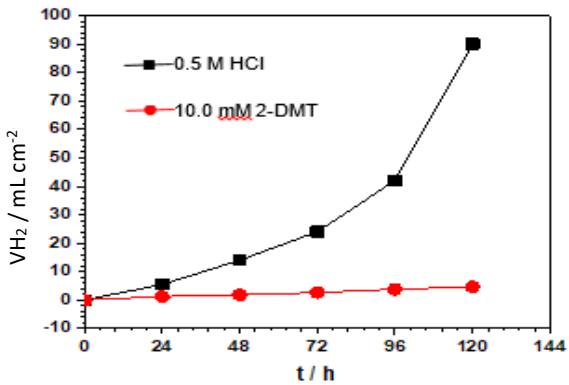


**Figure 5.** Hydrogen gas volume of MS electrode in 0.5 M HCI and with the existence of 10.0 mM 2-DMT after 120 h.

### 3.3. Thermodynamic Consideration

The most important event in the protection of the MS with the inhibitor is the adsorption of the inhibitor molecules on the metal surface. This event should be dealt with in detail. For this reason, in order to explain the adsorption process, several adsorption isotherms have been applied for this inhibitor and Langmuir isotherm provides the most suitable one. The plot of Langmuir isotherm ($C/\theta$ vs $C$) and related equation are given in Fig. 6. and below.

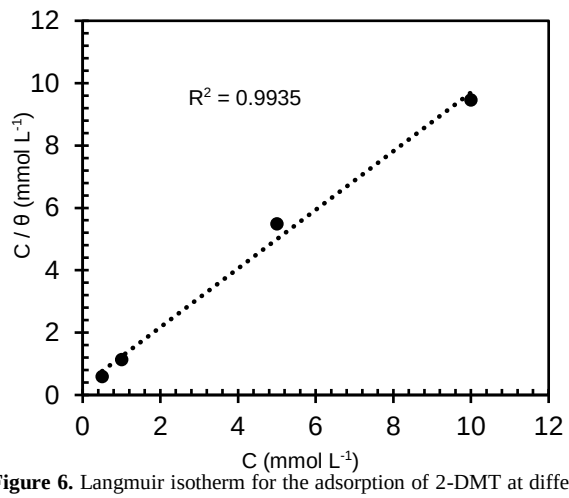


**Figure 6.** Langmuir isotherm for the adsorption of 2-DMT at different concentrations on the MS surface.

$$\frac{C_{(inh)}}{\theta} = \frac{1}{K_{(ads)}} + C_{(inh)} \quad (5)$$

$C_{inh}$, $\theta$ and $K_{ads}$ denote the concentration of inhibitor, degree of surface coverage and adsorption equilibrium constant, respectively. Intercept of equation 5 gives the $K_{ads}$ and its value is 3417 M$^{-1}$. This value is used for calculation of $\Delta G^o_{ads}$ in the following equation:

$$\Delta G^o_{ads} = -RT\ln(55.5K_{ads}) \quad (6)$$

$R$, $T$ and 55.5 denote the universal gas constant (8.314 J mol$^{-1}$ K$^{-1}$), temperature ($K$), and concentration $H_2O$, respectively. -30.11 kJ mol$^{-1}$ is found for $\Delta G^o_{ads}$. A negative sign shows the spontaneous adsorption and the value of $\Delta G^o_{ads}$ is between -20 kJ mol$^{-1}$ and -40 kJ mol$^{-1}$, indicating the mixed adsorption mode [33].

In addition to determining the adsorption process and calculating the thermodynamic parameters, a better understanding of the corrosion mechanism is required. We know that the adsorption of organic inhibitors to the metal surface occurs through electrostatic interactions [34]. In this study, to see whether there is an electrostatic interaction and to explain the inhibition mechanism, the surface charge of metal is measured using $E_{ocp}$ and $R_p$ with the existence of 10.0 mM 2-DMT and related figure is given below. The surface charge of metal is calculated as follows:

$$E_r = E_{ocp} - E_{pzc} \quad (7)$$

$E_r$ denotes the Antropov's rational corrosion potential [35]. $E_r$ is found to be 0.01 V (Ag/AgCI). This means that MS surface is charged with positive with the existence of inhibitor molecules. Mechanism can be described as follows: Negatively charged CI$^-$ ions can be adsorbed on positively charged MS surface at the firs step and the next step may be adsorption of the protonated inhibitor molecules [36]. Inhibitor molecules are protonated in the following way:

$$\text{2-DMT} + H^+ \leftrightarrow [\text{2-DMTH}]^+ \quad (8)$$

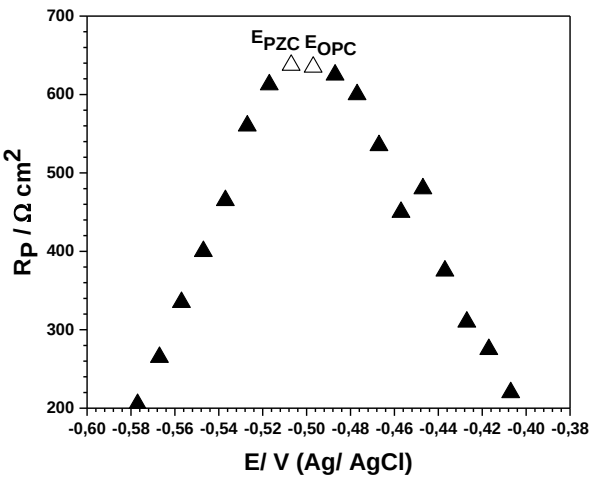


**Figure 7.** $R_p$ vs electrode potential for MS in 0.5 M HCl solution with the existence of 10 mM 2-DMT.

This electrostatic interaction (physical adsorption) forms a protective inhibitor film on the MS surface and this film prevents the metal from corrosion. In addition to the physical adsorption, functional groups such as amino, methyl and conjugated bonds lead to chemical adsorption on the MS surface, which contribute to the protective ability of inhibitor [34]. Same results are found in literature. For instance, a work by Gong et al. [37], inhibition abilities of 2-amino-4-(4-methoxyphenyl)-thiazole (MPT) and 2-amino-4-phenylthiazole (APT) were investigated for MS protection in acidic medium. $E_r$ values of these inhibitors are calculated positively, meaning that the surfaces of MS were positive charged after 1 h immersion. In another study, Ouakki et al. [38], investigated the corrosion inhibition performances of two organic compounds (2-(1,4,5-triphenyl-1H-imidazol-2-yl) phenol (P1) and 3-methoxy-4-(1,4,5-triphenyl-1H-imidazol-2-yl) phenol (P2)) for MS in 1.0 M HCl. Results showed that $CI^-$ ions will be the first to adsorb on MS surface and inhibitor in cationic form interacts with ions.

### 3.4. Surface Morphology Results

Figure 8 shows the SEM and AFM images of MS electrode in 0.5 M HCI and with the existence of 10.0 mM 2-DMT after 120 h. It is seen that MS surface is intensely corroded by acid environment after 120 h. Islands and cavities formed over the surface. Fortunately, as shown in Fig. 8c, the surface structure of the MS is smooth and some corrosion products are seen after adding 2-DMT. AFM images support the SEM results. Average roughness of bare MS and after adding 2-DMT are found to be 138.3 nm and 39.6 nm, respectively. As a result, 2-DMT significantly inhibited the MS corrosion in HCI environment.

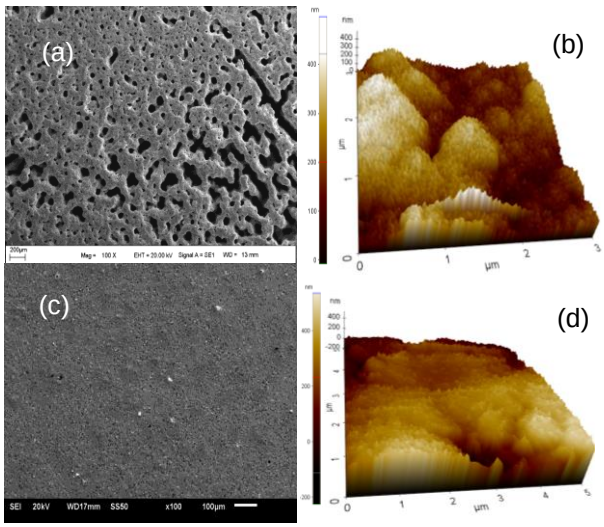


**Figure 8.** SEM (a,c) and 3D AFM (b,d) images of MS electrode in 0.5 M HCI (a,b) and with the existence of 10.0 mM 2-DMT (c,d) after 120 h.

### 3.5. Quantum Chemical Calculation Results

In addition to electrochemical experiments, quantum chemical calculation is performed to better understand the relationship between structural, electronic properties and adsorption process. Figure 9 depicts the structure of 2,4-Diamino-6-methly-1, 3, 5-triazine (2-DMT). B3LYP was used on the basis of DFT with a tuned of 6-311 ++ G (d, p) to obtain these geometries. Corrosion inhibitors have been extensively researched in heterocyclic chains, carboxyl, amines, conjugated bonds, and electronegative atom (N) [39-45]. These groups, according to the findings, acted as specific adsorption centres and rose to prominence. While the inhibitor mechanism anticorrosion inhibition is not fully understood, it can be stated that the inhibitor, in general, tends to offer electrons to the metal's unoccupied d orbital, and this trend increases as the magnitude of the orbital's energy of HOMO increases [46]. The values of absolute hardness ($\eta$), absolute electronegativity ($\chi$), fraction of transferred electrons ($\Delta N$) and absolute softness ($\sigma$) were calculated [47-52];

$$\Delta E = E_{LUMO} - E_{HOMO} \quad (9)$$

$$A = -E_{LUMO} \quad (10)$$

$$I = -E_{HOMO} \quad (11)$$

$$\eta = \frac{1}{2}(I - A) \quad (12)$$

$$\sigma = \frac{1}{\eta} \quad (13)$$

$$\chi = \frac{1}{2}(I + A) \quad (14)$$

$$\Delta N = \frac{\chi Fe - \chi inh}{2(\eta Fe + \eta inh)} \quad (15)$$



Table 4 shows the calculated parameters for this study, and Figure 9 shows the orbitals. The HOMO energy was -7.1980, as shown in Table 4. The HOMO was usually found in 2-DMT zones including atoms of N and a ring of heterocyclic. The energy of the LUMO was -1.9959 eV. The HOMO was discovered on the N terminals of the 2-DMT. In Table 4, the values for electronegativity were 4.5969 eV, hardness was 2.6010 eV, and softness was 0.3844. Adsorption appears to be appropriate for the interplay among not shared electron pairs of N atoms, electrons of the heterocyclic ring, and the metal's unoccupied d orbital. The molecules efficiency was also determined by examining the parameters of global reactivity. The energy gap ($\Delta E$) reflected the inhibitor molecule's reactivity to the metal. A low $\Delta E$ value indicated strong metal adsorption with high inhibitive efficiency. As the $\Delta E$ value decreases, the reactivity and tendency of electron donation increases. The dipole moment (3.1062 D) value can give an idea of the probability of the adsorption of molecules. The increased dipole moment could be attributed to dipole-dipole interactions between the molecules of inhibitor and the surface of the metal, resulting in increased inhibition. The processes of electron sharing between the inhibitor and the surface of metal can be argued as functions at the value $\Delta N$ listed in Table 4 with respect to Pearson theory [53]. The process of electron transfer is with respect to the electronegativity value ($\chi$), as well as the lower electronegativity as well as the higher transfer of electron. The fraction of electrons transferred, $\Delta N$

(0.4619) is important parameter to investigate corrosion inhibition. In the literature, it is claimed that high $\Delta N$ value help promote high adsorption to the MS surface, which is good inhibition and protection [53]. If $\Delta N$ is greater than zero, electrons move from inhibitors to the surface of metal atoms; otherwise, electrons move from the surface of the metal to molecules of the inhibitor [39, 54]. The inhibition efficiency and quantum parameters have a strong correlation.

**Table 4.** DFT/B3LYP/6-311G (++ d,p) method calculated quantum parameters for 2-DMT.

| Inhibitor | $E_{HOMO}$ (eV ) | $E_{LUMO}$ (eV) | $\Delta E$ (eV) | $\beta$ (eV) | $\gamma$ (eV) | $S$ (eV$^{-1}$) | $\Delta N$ | $\mu$ (Debye) |
|---|---|---|---|---|---|---|---|---|
| **2-DMT** | -7.1980 | -1.9959 | 5.2021 | 4.5969 | 2.6010 | 0.3844 | 0.4619 | 3.1062 |

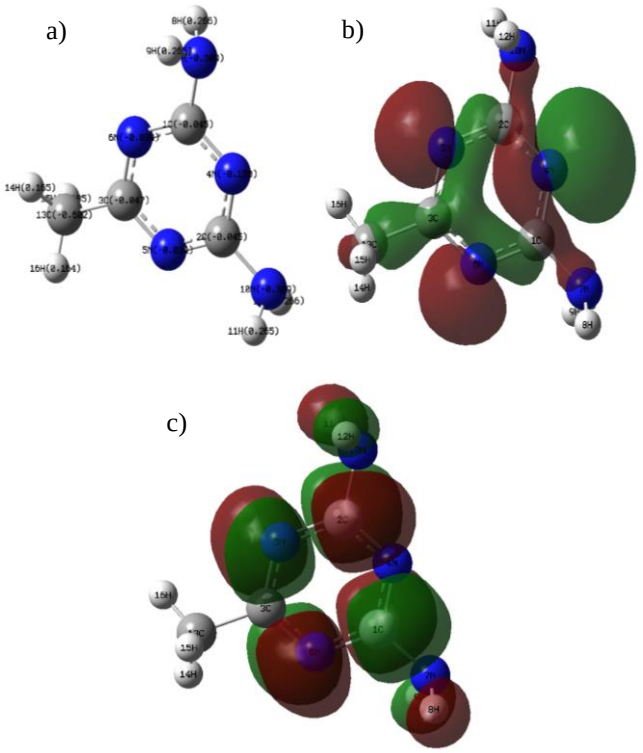


**Figure 9.** 2-DMT molecule structures with Mulliken charge (a), HOMO (b), and LUMO (c) orbitals.

## 4. CONCLUSION

A new organic compound as a corrosion inhibitor is studied for MS protection from acid corrosion using electrochemical, morphological and quantum chemical calculation methods. Following results can be drawn:

1. Tafel curves (cathodic and anodic) and Langmuir adsorption isotherm (physical and chemical adsorption) show that studied inhibitor is classified as mixed-type. Tafel curves do not change with the existence of different concentrations of 2-DMT in blank solution, implying that the same corrosion mechanism occurs in both corrosive media due to giving parallel lines.
2. While values of $i_{corr}$ decreased, $R_p$ values increased with the existence of 0.5, 1.0, 5.0 and 10.0 mM 2-DMT, indicating that a stable inhibitor film formed on the MS surface and this film behaves like a preventative.
3. The protection ability of some triazine-containing compounds are compared with 2,4-Diamino-6-methly-1,3,5-triazine and inhibition efficiency of studied inhibitor in this study is found higher than those of the previous studied inhibitors. This promising result once again exhibits the importance of this class of compounds for protecting metals in an acidic medium.
4. Although the diameter of semicircles of both bare MS and with the existence of 10.0 mM 2-DMT decreased after 120 h, the corrosion rate of MS electrode with the existence of 10.0 mM 2-DMT is slower than that of bare MS and very low hydrogen gas is obtained on the MS electrode with the existence of 10.0 mM 2-DMT.
5. The adsorption of inhibitor molecules on the MS surface is discussed in more detail and the existence of electrostatic and chemical interactions are confirmed by PZC results.
6. -30.11 kJ mol$^{-1}$ is found for $\Delta G^o_{ads}$. Negative sign shows the spontaneous adsorption.
7. SEM and AFM images confirm the existence of inhibition by 2-DMT due to obtaining smooth surface.
8. Quantum chemical calculation manifested that adsorption ability of inhibitor molecule is due to dipol moment and high value of $\Delta N$.



**Acknowledgement**

I would like to thank Mardin Artuklu University for supporting this study.

## REFERENCES

[1] Koch G, Trends in oil and gas corrosion research and technologies. 1st ed. Elsevier Inc.; 2017.
[2] Rodriguez-Alonso L, Lopez-Sanchez J, Serrano A, de la Fuente OR, Galvan JC, Carmona N. Hybrid sol-gel coatings doped with non-toxic corrosion inhibitors for corrosion protection on AZ61 magnesium alloy. Gels 2022;8(34):1-12.
[3] Ouyang Y, Li LX, Xie ZH, Tang L, Wang F, Zhong CJ. A self-healing coating based on facile pH-responsive nanocontainers for corrosion protection of magnesium alloy. J. Magnes. Alloy. 2022;10:836-49.
[4] Jiang Y, Gao S, Liu Y, Huangfu H, Guo X, Zhang J. Enhancement of corrosion resistance of AZ31B magnesium alloy by preparing MgAl-LDHs coatings modified with imidazolium based dicationic ionic liquid, Surf Coating Technol 2022;440:128504.
[5] Tan B, Lan S, Zhang S, Deng H, Qiang Y, Fu A, Ran Y, Xiong J, Marzouki R, Li W. Passiflora edulia Sims leaves Extract as renewable and degradable inhibitor for copper in sulfuric acid

solution. Colloids Surfaces A Physicochem. Eng. Asp. 2022;645:128892.

[6] Sefaja J, Dernikovic B, Malina J, Lovrecek B. Investigation of steel corrosion in pickling solutions: Solutions with inhibitors. Surf. Technol. 1983;20(3):247–63.

[7] Goyal M, Kumar S, Bahadur I, Verma C, Ebenso E.E. Organic corrosion inhibitors for industrial cleaning of ferrous and non-ferrous metals in acidic solutions: A review. J. Mol. Liq. 2018;256:565–73.

[8] Yıldız R. An electrochemical and theoretical evaluation of 4,6-diamino-2-pyrimidinethiol as a corrosion inhibitor for mild steel in HCl solutions. Corrosion Sci. 2015;90:544-53.

[9] Ech-chihbi E, Nahl A, Salim R, Benhiba F, Moussaif A, El-Hajjaji F, et al. Computational, MD simulation, SEM/EDX and experimental studies for understanding adsorption of benzimidazole derivatives as corrosion inhibitors in 1.0 M HCl solution. J. Alloys Compd. 2020;844:155842.

[10] Fakhry H, El Faydy M, Benhiba F, Laabaissi T, Bouassiria M, Allali M, et al. A newly synthesized quinoline derivative as corrosion inhibitor for mild steel in molar acid medium: Characterization (SEM/EDS), experimental and theoretical approach. Colloids Surf, A Physicochem Eng Asp 2021:610:125746.

[11] Yıldız R, Döner A, Doğan T, Dehri İ. Experimental studies of 2-pyridinecarbonitrile as corrosion inhibitor for mild steel in hydrochloric acid solution. Corros. Sci. 2014;82:125-32.

[12] Ganapathi Sundaram R, Sundaravadivelu M. Anticorrosion activity of 8-quinoline sulphonyl chloride on mild steel in 1 M HCl solution. J. Metall 2016;8095206.

[13] Xhanari K, Finsgar M. Organic corrosion inhibitors for aluminium and its alloys in acid solutions: A review. RSC Adv. 2016;6(67):62833–57.

[14] Döner A, Kardaş G. N-Aminorhodanine as an effective corrosion inhibitor for mild steel in 0.5 M $H_2SO_4$. Corrosion Sci. 2011;53:4223–32.

[15] El-Faham A, Osman SM, Al-Lohedan HA, El-Mahdy GA. Hydrazino-methoxy-1,3,5-triazine derivatives' excellent corrosion organic inhibitors of steel in acidic chloride solution. Molecules 2016;21(6):714.

[16] Arshad M, Khan TA, Khan MA. 1,2,4-triazine derivatives: Synthesis and biological applications. Int. J. Pharm. Sci. 2014;5(4):149-62.

[17] Zarrok H, Oudda H, El Midaoui A, Zarrouk A, Hammouti B, Ebn Touhami M, Attayibat A, Radi S, Touzani R, Some new bipyrazole derivatives as corrosioninhibitors for C38 steel in acidic medium, Res. Chem. Intermed. 2012;38(8):2051–63.

[18] Bououidina A, Ech-chihbi E, El-Hajjaji F, El Ibrahimi B, Kaya S, Taleb M, Anisole derivatives as sustainable-green inhibitors for mild steel corrosion in 1 M HCl: DFT and molecular dynamic simulations approach. J. Mol. Liq. 2021;324:115088.

[19] Murulana LC, Kabanda MM, Ebenso EE. Experimental and theoretical studies on the corrosion inhibition of mild steel by some sulphonamides in aqueous HCl. RSC Adv. 2015;36:28743–61.

[20] Li X, Deng S, Lin T, Xie X, Du G. 2-Mercaptopyrimidine as an effective inhibitor for the corrosion of cold rolled steel in $HNO_3$ solution. Corros. Sci. 2017;118:202-16.

[21] Li Y, Zhang S, Ding Q, Qin B, Hu L. Versatile 4, 6-dimethyl-2-mercaptopyrimidine based ionic liquids as high-performance corrosion inhibitors and lubricants. J. Mol. Liq. 2019;284:577–85.

[22] Seung-Hyun Y, Young-Wun K, Chung K, Nam-Kyun K, Joon-Seop K. Corrosion inhibition properties of triazine derivatives containing carboxylic acid and amine groups in 1.0 M HCl solution. Ind. Eng. Chem. Res. 2013;52(32):10880–89.

[23] Nassar IM, Abbas MA, Hamdy A, Elazabawy OE, Evaluating the inhibiting action of cds nanoparticles and cds/pmma hybrid for corrosion of carbon steel in acidic media, international journal of current research 2013;5:4327–37.

[24] Haque J, Ansari KR, Srivastava V, Quraishi MA, Obot IB. Pyrimidine derivatives as novel acidizing corrosion inhibitors for N80 steel useful for petroleum industry: A combined experimental and theoretical approach. J Ind Eng Chem, 2017;49:176-88.

[25] Ichchou I, Larabi L, Rouabhi H, Harek Y, Fellah A. Electrochemical evaluation and DFT calculations of aromatic sulfonohydrazides as corrosion inhibitors for XC38 carbon steel in acidic media. J. Mol. Struct. 2019;1198:126898.

[26] Singh P, Singh A, Quraishi MA. Inhibition effect of 1,3,5-tri-p-tolyl-1,3,5-triazene on the corrosion of brass in 0.5 M HCl solution. Res Chem Intermed 2014;40:595–4

[27] Migahed M, Nassar I. Corrosion inhibition of tubing steel during acidization of oil and gas wells. Electrochim. Acta 2008;53:2877–82.

[28] Yadav M, Kumar S, Tiwari N, Bahadur I, Ebenso EE. Experimental and quantum chemical studies of synthesized triazine derivatives as an efficient corrosion inhibitor for N80 steel in acidic medium. J. Mol. Liq. 2015;212:151–67.

[29] John S, Joseph A, Sajini T, Jose AJ. Corrosion inhibition properties of 1,2,4-Hetrocyclic systems: Electrochemical, theoretical and Monte Carlo simulation studies. Egypt. J. Pet. 2017;26:721–32.

[30] Salman M, Ansari KR, Haque J, Srivastava V, Quraishi MA, Mazumder MAJ, Ultrasound-assisted synthesis of substituted triazines and their corrosion inhibition behavior on N80 steel/acid interface. J Heterocyclic Chem. 2020;57:2157–72.

[31] Shukla SK, Singh AK, Quraishi MA. Triazines: Efficient corrosion inhibitors for mild steel in hydrochloric acid solution. Int. J. Electrochem. Sci. 2012;7:3371 – 89.

[32] Usman BJ, Gasem ZM, Umoren SA, Solomon MM. Eco-friendly 2-Thiobarbituric acid as a corrosion inhibitor for API 5L X60 steel in simulated sweet oilfield environment: Electrochemical and surface analysis studies. Scientific Reports, 2019;9:830.

[33] Gurjar S, Ratnani S, Kandwal P, Tiwari KK, Sharma A, Sharma SK. Experimental and theoretical studies of 1-Benzyl pyridazinium bromide as green inhibitor for mild steel corrosion. e-Prime - Advances in Electrical Engineering, Electronics and Energy 2022;2:100054.

[34] Shao H, Yin X, Zhang K, Yang W, Chen Y, Liu Y. N-[2-(3-indolyl)ethyl]-cinnamamide synthesized from cinnamomum cassia presl and alkaloid tryptamine as green corrosion inhibitor for Q235 steel in acidic medium. J. Mater. Res. Technol. 2022;20:916-33.

[35] Fuchs-Godec R. The adsorption CMC determination and corrosion inhibition of some N-alkyl quaternary ammonium salts on carbon steel surface in 2M $H_2SO_4$. Colloids Surf. A Physicochem. Eng. Aspects 2006;280:130–39.

[36] Kaya F, Solmaz R, Geçibesler İH. Adsorption and corrosion inhibition capability of Rheum ribes root extract (Işgın) for mild steel protection in acidic medium: A comprehensive electrochemical, surface characterization, synergistic inhibition effect, and stability study. J. Mol. Liq. 2023;372:121219.

[37] Gong W, Yin X, Liu Y, Chen Y, Yang W. 2-Amino-4-(4-methoxyphenyl)-thiazole as a novel corrosion inhibitor for mild steel in acidic medium. Progress in Organic Coatings 2019;126:150–61.

[38] M. Ouakki, M. Galai, M. Rbaa, Ashraf S. Abousalemd, B. Lakhrissi, M. Ebn Touhami, M. Cherkaoui, Electrochemical, thermodynamic and theoretical studies of some imidazole derivatives compounds as acid corrosion inhibitors for mild steel. J. Mol. Liq. 2020;319:114063.

[39] Alamiery A, A.B. Mohamad, A.A.H. Kadhum, M.S. Takriff. Comparative data on corrosion protection of mild steel in HCl using two new thiazoles. Data Brief 2022;40:107838.

[40] Wang C, Zou C, Cao Y. Electrochemical and isothermal adsorption studies on corrosion inhibition performance of β-cyclodextrin grafted polyacrylamide for X80 steel in oil and gas production. J. Mol. Struct. 2021;1228:129737.

[41] Ferraa S, Ouakki M, Barebita H, Nimour A, Cherkaoui M, Guedira T. Corrosion inhibition potentials of some phosphovanadate-based glasses on mild steel in 1 M HCl. Inorg. Chem. Commun. 2021;132:108806.

[42] El-Zekred MA, Nofal AM, Shalabi K, Fouda AS. Ficus carica extract as environmentally friendly inhibitor for the corrosion of L-80 carbon steel in 0.5 M $H_2SO_4$ media, J. Indian Chem. Soc. 2021;98.100128.

[43] Costa SN, Almeida-Neto FWQ, Campos OS, Fonseca TS, de Mattos MC, Freire VN., et al. Carbon steel corrosion inhibition in acid medium by imidazolebased molecules: Experimental and molecular modelling approaches. J. Mol. Liq. 2021;326:115330.

[44] Abdallah M, Gad EAM, Sobhi M, Al-Fahemi JH, Alfakeer MM. Performance of tramadol drug as a safe inhibitor for aluminum corrosion in 1.0 M HCl solution and understanding mechanism of inhibition using DFT. Egypt J. Pet. 2019;28:173–81.

[45] Sığırcık G, Yıldırım D, Tüken T. Synthesis and inhibitory effect of N,N'-bis(1-phenylethanol)ethylenediamine against steel corrosion in HCl Media. Corrosion Sci. 2017;120:184–93.

[46] Pour-Ali S, Hejazi S. Tiazofurin drug as a new and non-toxic corrosion inhibitor for mild steel in HCl solution: experimental and quantum chemical investigations. J. Mol. Liq. 2022;354:118886.

[47] Hegazy MA, Atlam FM. Three novel bolaamphiphiles as corrosion inhibitors for carbon steel in hydrochloric acid: Experimental and computational studies. J Mol. Liq. 2016;218:649–62.

[48] Yıldız R. Adsorption and inhibition effect of 2,4-diamino-6-hydroxypyrimidine for mild steel corrosion in HCl medium: experimental and theoretical investigation. Ionics 2019; 25:859–70.

[49] Verma C, Quraishi M, Singh A. 2-Amino-5-nitro-4, 6-diarylcyclohex-1-ene-1, 3, 3- tricarbonitriles as new and effective corrosion inhibitors for mild steel in 1 M HCl: Experimental and theoretical studies, J. Mol. Liq. 2015;212:804–12.

[50] Yıldız R, Doğru Mert B. Theoretical and Experimental Investigations on Corrosion Control of Mild Steel in Hydrochloric Acid Solution by 4-aminothiophenol. Anti-Corros Meth Mater. 2019;66:127–37.

[51] Keleşoğlu A, Yıldız R, Dehri İ, 1-(2-Hydroxyethyl)-2 Imidazolidinone as corrosion inhibitor of mild steel in 0.5 M HCl solution: thermodynamic, electrochemical and theoretical studies. J Adhes Sci Technol 2019;33:2010–30.

[52] Keleşoğlu A, Sığırcık G, Yıldız R, Dehri İ. Experimental and theoretical investigation of Pyrazinecarboxamide against mild steel corrosion. J Dispers Sci Technol 2023;44(2):329–341.

[53] Gomez B, Likhanova N, Dominguez-Aguilar M, Martinez-Palou R, Vela A, Gazquez JL. Quantum chemical study of the inhibitive properties of 2-pyridyl-azoles, J. Phys. Chem. B. 2006;110:8928-34.

[54] Tüzün B, Bhawsar J. Quantum chemical study of thiaozole derivatives as corrosion inhibitors based on density functional theory, Arab. J. Chem. 2021;14(2): 102927.